Artificial Intelligence In Medicine 144 (2023) 102646

Contents lists available at ScienceDirect

Artificial Intelligence In Medicine

journal homepage: www.elsevier.com/locate/artmed

Research paper

Automated estimation of mitral annular plane systolic excursion by artificial intelligence from 3D ultrasound recordings

Anders Austlid Taskén [a,*], Erik Andreas Rye Berg [b,c], Bjørnar Grenne [b,c], Espen Holte [b,c], Håvard Dalen [b,c,d], Stian Stølen [b,c], Frank Lindseth [a], Svend Aakhus [b,c], Gabriel Kiss [a]

[a] Department of Computer Science, Faculty of Information Technology and Electrical Engineering, Norwegian University of Science and Technology, Høgskoleringen 1, 7491 Trondheim, Norway
[b] Department of Circulation and Medical Imaging, Faculty of Medicine and Health Sciences, Norwegian University of Science and Technology, Norway
[c] Clinic of Cardiology, St. Olavs University Hospital, Trondheim, Norway
[d] Levanger Hospital, Nord-Trøndelag Hospital Trust, Levanger, Norway

ARTICLE INFO

Keywords:
Convolutional neural network
Landmark detection
Cardiac monitoring
MAPSE
Ultrasound
Echocardiography

ABSTRACT

Perioperative monitoring of cardiac function is beneficial for early detection of cardiovascular complications. The standard of care for cardiac monitoring performed by trained cardiologists and anesthesiologists involves a manual and qualitative evaluation of ultrasound imaging, which is a time-demanding and resource-intensive process with intraobserver- and interobserver variability. In practice, such measures can only be performed a limited number of times during the intervention. To overcome these difficulties, this study presents a robust method for automatic and quantitative monitoring of cardiac function based on 3D transesophageal echocardiography (TEE) B-mode ultrasound recordings of the left ventricle (LV). Such an assessment obtains consistent measurements and can produce a near real-time evaluation of ultrasound imagery. Hence, the presented method is time-saving and results in increased accessibility. The mitral annular plane systolic excursion (MAPSE), characterizing global LV function, is estimated by landmark detection and cardiac view classification of two-dimensional images extracted along the long-axis of the ultrasound volume. MAPSE estimation directly from 3D TEE recordings is beneficial since it removes the need for manual acquisition of cardiac views, hence decreasing the need for interference by physicians. Two convolutional neural networks (CNNs) were trained and tested on acquired ultrasound data of 107 patients, and MAPSE estimates were compared to clinically obtained references in a blinded study including 31 patients. The proposed method for automatic MAPSE estimation had low bias and low variability in comparison to clinical reference measures. The method accomplished a mean difference for MAPSE estimates of (-0.16 ± 1.06) mm. Thus, the results did not show significant systematic errors. The obtained bias and variance of the method were comparable to inter-observer variability of clinically obtained MAPSE measures on 2D TTE echocardiography. The novel pipeline proposed in this study has the potential to enhance cardiac monitoring in perioperative- and intensive care settings.

1. Introduction

The clinical standard for perioperative evaluation of heart function is based on vital signs and clinical observations. This conventional monitoring consists of measurements of blood pressure, heart rate, and arterial oxygen saturation, and is imperative in the event of severe illness. Nonetheless, the clinical care standard lacks direct monitoring of heart function.

Surveillance of heart function by echocardiography can enhance diagnosis accuracy and positively impact clinical decision-making [1, 2]. Transesophageal echocardiography is a valuable and highly used technique for the perioperative evaluation and monitoring of LV function [3] and is in recent times widely adopted in the operating theatre. Since the ultrasound probe is placed in the esophagus during surgery, the transducer is close to the heart and provides high-quality imaging of anatomical cardiac structures. Additionally, since the probe is situated stationary in the esophagus after placement, TEE acquisitions may require less manipulation by the clinicians during interventions compared to standard transthoracic echocardiogram (TTE).

* Corresponding author.
E-mail addresses: anders.a.tasken@ntnu.no (A.A. Taskén), erik.a.berg@ntnu.no (E.A.R. Berg), bjornar.grenne@ntnu.no (B. Grenne), espen.holte@ntnu.no (E. Holte), havard.dalen@ntnu.no (H. Dalen), stian.stolen@ntnu.no (S. Stølen), frankl@ntnu.no (F. Lindseth), svend.aakhus@ntnu.no (S. Aakhus), gabriel.kiss@ntnu.no (G. Kiss).

https://doi.org/10.1016/j.artmed.2023.102646
Received 28 September 2022; Received in revised form 22 August 2023; Accepted 28 August 2023
Available online 31 August 2023

Cardiologists or anesthesiologists assess LV systolic and diastolic function by discrimination of the continuous imaging acquired by TEE. LV function is estimated by visual appraisal of myocardial deformation and excursion, as well as time-consuming quantitative analysis. The clinical value and usage of LV monitoring by visual inspection of TEE imaging is, nevertheless, restricted by four drawbacks:

1. Qualitative measures are dependent on subjective visual evaluations, which results in observer variability.
2. Visual inspection of echocardiographic images is a procedure of high complexity performed by experts, thus deviating the cardiologist's or anesthesiologist's focus from other imminent assignments during interventions.
3. Repeated manual evaluation of imagery by experts is expensive in terms of both expert resources and hospital costs.
4. Due to the plenitude of acute tasks during interventions, the clinical use of LV monitoring is strongly restricted or not practically feasible.

Automatic estimation of LV function based on TEE imagery may therefore be highly valuable for perioperative monitoring. Automatic estimation of global LV function possesses the potential to increase both the clinical usage and diagnostic value of cardiac monitoring. Increased use of LV function surveillance in general intensive care settings may benefit patients with heart failure, myocardial infarction, hypertrophic cardiomyopathy, aortic stenosis, atrial fibrillation, or other severe illnesses [4,5].

MAPSE is a robust measure of global LV longitudinal function and depends on contractility and load [6]. MAPSE is a parameter with high reproducibility and low dependence on image quality [7], and is proven to be a useful parameter for assessment of LV longitudinal function [8–10]. It has a high correlation with global longitudinal strain (GLS) [11], and is suggested as a surrogate for LV ejection fraction (LVEF) [12]. Since the apex is not always clearly visualized in TEE recordings, MAPSE estimation results in increased feasibility and robustness compared to the estimation of LVEF. MAPSE is shown to possess a high correlation with cardiovascular pathology when the cardiac longitudinal function is affected, for instance, coronary artery disease, myocardial infarction, and dilated cardiomyopathy [9,13–15]. Reflecting the impaired longitudinal shortening, MAPSE is a sensitive early marker of systolic dysfunction in LV hypertrophy, while LVEF may remain preserved in the same situation [9,16,17]. Hence, automatic estimation of MAPSE through TEE recordings could be valuable for perioperative cardiac monitoring. MAPSE is therefore the chosen focus area of this study.

1.1. Related works

Automated estimation of physiological parameters describing heart function has been employed in numerous studies earlier. Nordal [18] obtained a pipeline for MAPSE prediction on two-dimensional TEE ultrasound images with mid-esophageal two chamber- (2C) and four chamber (4C) views, with a mean difference of (-0.08 ± 1.38) mm compared to clinically obtained measures. The proposed method proved a promising potential for the use of machine learning in automated MAPSE estimation. Nonetheless, the study contained limitations due to the dependence on high-quality mid-esophageal 2C- and 4C echocardiographic images, and uncertainty in estimates by virtue of a small dataset in both training and validation of the method. Storve et al. [19] and Grue et al. [20] presented an approach for the detection of LV dysfunction from color tissue Doppler apical four-chamber recordings with MAPSE estimation. Grue et al. found that MAPSE $\leq$ 10 mm detected LV dysfunction with a sensitivity of 82% and a specificity of 76%. The method is designed for transthoracic echocardiograms, and thus less applicable for monitoring purposes.

Automatic alignment of 3D ultrasound volumes has been proven possible through earlier publications. Orderud et al. [21] presented a method for TTE data based on segmentation of the LV using a coupled deformable model. Landmarks extracted from the segmentation, corresponding to the apex and base, were used to align the volume. Such an approach is not suitable for the TEE data available in this study, since the apex is barely visible in the acquisitions. Veronesi et al. [22] suggested a method for alignment based on long-axis measurements through optical flow, but the pipeline was dependent on manual interaction by the operator and thus not suited for a fully automatic method.

3D segmentation and modeling of the mitral valve from 3D ultrasound recordings for evaluation of mitral valve (MV) morphology have been proven possible in earlier studies [23–26]. Similarly, a set of studies have performed localization of the mitral annulus from 3D TEE data for detection or tracking of the mitral ring shape and motion, and for transcatheter MV repair guidance [27–30]. Fully automatic deep learning-based segmentation of the mitral annulus with TEE ultrasound acquisitions has previously been completed by Nordal [18] and Andreassen et al. [31] with promising accuracy, for 2D and 3D data. Classification of standard cardiac views in 2D and 3D TTE imagery based on a convolutional neural network was proposed by Østvik et al. [32]. The published method included an original and lightweight CNN with real-time performance. The mitral annulus segmentation applied in the current study is a continuation of the works presented by Nordal [18] and Andreassen et al. [31], and the view classification applied in the current study is completed with a modified version of the CNN proposed by Østvik et al. [32]. The resulting pipeline provides fully automatic MAPSE estimations on 3D TEE imagery, with no need for assistance or probe adjustments.

1.2. Objectives

The overall research goal is to develop and establish a robust non-harming method for automatic cardiac monitoring of global LV function. Since the ultrasound probe must be in a neutral position during a perioperative cardiac monitoring setting due to patient hazard, the method must handle varying image quality. To achieve the aim of the study, volume alignment, 3D segmentation of the mitral annulus and classification of standardized cardiac views from 3D echocardiography recordings are obtained and MAPSE is estimated through a set of post-processing computations. Since the pipeline is based on 3D TEE ultrasound recordings, the method is fully automatic, and no inference by a physician is needed. The accuracy of the proposed methodology is evaluated by comparison of estimates to clinical measures and state-of-the-art methods.

2. Materials and method

2.1. Dataset and pre-processing

The dataset used in the development and evaluation of the method is 3D TEE B-mode ultrasound images from the Echocardiography Unit, Clinic of Cardiology at St. Olavs University Hospital in Trondheim, Norway. The imaging was performed by cardiologists with expertise in echocardiography. The scanners used to obtain the TEE data were clinical scanners named GE Vivid E95. A 6VT-D probe was used for recording purposes, provided by GE Vingmed, Horten, Norway. The depth and angle of the ultrasound sector were adjusted such that the entire LV was visualized. The frame rate of the acquired data varied from 4 to 36 frames per second (FPS), with a mean of 15 FPS. The ultrasound probe was in a neutral position during acquisition to mimic conditions present in the operating room (OR) during monitoring. Hence, the available data are subject to a significant amount of foreshortening and variable image quality compared to standard echocardiograms. Additionally, respiratory movement of the heart is present. 3D TEE echocardiography from a total of 107 patients were included in the study. Several recordings were acquired for each patient, resulting in a

Table 1
Overview of the 3D TEE dataset.

	Train/Validate	Test
Patients	76	31
Recordings	197	65
Frames	2448	855
Extracted images annotated for volume alignment	258 840	81 360
Extracted images annotated for view classification	395 280	131 580

total of 262 ultrasound recordings. Each recording included 3 cardiac cycles in total.

The dataset was divided into a train set and a test set, as presented in Table 1. The train set was used for training and validation of the networks related to volume alignment and cardiac view classification, and the test set was utilized to evaluate the volume alignment, cardiac view classification and MAPSE estimation. A total of 33 out of the 262 recordings were excluded from the volume alignment dataset due to insufficient image quality after evaluation by clinical experts. 25 out of the 262 recordings were excluded from the dataset used for cardiac view classification for similar reasons.

The collection and analyses of the ultrasound data were completed with both informed patient consent and approval from the Regional Committee for Medical and Health Research Ethics (REK) at St. Olavs University Hospital. Consecutive patients scheduled for a routine exam at the echo lab were included in the study. Hence, there was no patient selection. The underlying cause of examination for the included patients was related to a wide specter of cardiac diseases. No data selection based on the diagnosis was performed. The obtained dataset is therefore a simple random sample from a population being examined at an echo lab with secondary care for the region.

The acquired data were anonymized, and the raw ultrasound beam data were converted from the proprietary DICOM files and scan-converted to isotropic 3D images by applying a polar to Cartesian transformation. The Cartesian image data were exported to a set of HDF5 files, together with metadata of the corresponding geometric information and acquisition parameters.

MAPSE reference values for 3D recordings of all patients in the test set were derived by cardiologists with expertise in echocardiography in the clinically approved software named EchoPac (GE Vingmed Ultrasound, Horten, Norway). The reference MAPSE values were constructed with the use of 2C-, 4C-, and long-axis (LAX) views, and two recordings were utilized per patient. This resulted in a total of 62 recordings with MAPSE references. All clinically obtained references were used in the study to evaluate the model. Since EchoPac does not offer a dedicated 3D MAPSE measurement tool, the MAPSE parameter was determined in EchoPac by indicating the point on the standard planes corresponding to the intersection with the mitral annulus. This procedure was completed for the frames with the maximum and minimum position of the annulus along the long-axis, per cardiac cycle. Hence, clinical MAPSE reference measures were obtained for inferoseptal- and anterolateral mitral annular points in 4C views, inferior and anterior mitral annular points in 2C views, and inferolateral mitral annular points in LAX views. The anteroseptal basal points from the LAX view was discarded since these measures are error-prone due to a lack of clear mitral annulus points in the presence of the LV outflow tract (LVOT), and since it is common to avoid measuring MAPSE in these sectors in the clinic [33]. Screenshots of EchoPac are given in Fig. 1 to visualize how the reference MAPSE measures were obtained.

2.2. Pipeline

The complete pipeline of the proposed method is visualized in Fig. 2. The 3D TEE ultrasound volumes were aligned automatically along the long-axis with a novel method based on machine learning to avoid foreshortened slices, geometric distortion and out-of-plane

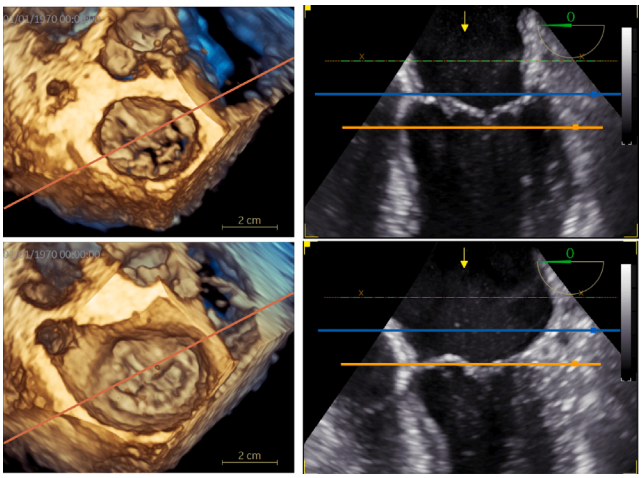

Fig. 1. Screenshots from EchoPac used to obtain MAPSE reference measures. A 3D render of the mitral valve is given on the left side, where the red line indicates the slice used to produce the 2D images on the right. End-diastole (ED) is given in the two upper images, and end-systole (ES) in the bottom two images. The horizontal lines on the 2D slices indicates the annulus excursion of the inferoseptal segment, and gives the MAPSE reference for the given segment. (For interpretation of the references to color in this figure legend, the reader is referred to the web version of this article.)

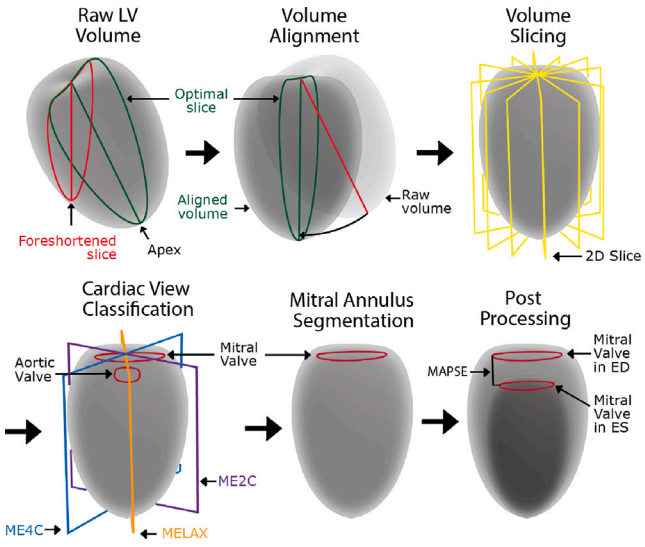

Fig. 2. Visualization of the MAPSE estimation pipeline.

movement. 2C-, 4C- and LAX views were automatically classified for a complete orientation of the volume by a neural network, and to obtain segmented MAPSE measures for clinical comparison. A discrete 3D segmentation of the mitral annulus was obtained by landmark detection based on deep learning for each frame in the recording, and a set of post-processing computations was conducted to estimate global and segmental MAPSE measures.

2.3. Volume slicing

Two-dimensional slices of the volumetric ultrasound recordings were extracted by a GPU-accelerated method based on vectorization to directly compute the indices. Given an ultrasound volume, defined by Eq. (1), an image plane rotated θ degrees about the z-axis were extracted by calculating the corresponding indices I with the Einstein summation convention according to Eq. (2). Images extracted by rotation about the x- or y-axis were obtained with a similar method, by

replacing the rotation matrix $\boldsymbol{R}(\theta)$ and the matrices $\boldsymbol{P}_i$ for $i \in [0, 1, 2]$.

$$\boldsymbol{V} = \{(x, y, z) | x \in [0, s_x], y \in [0, s_y], z \in [0, s_z]\} \tag{1}$$

$$\boldsymbol{I}_{i,j,k}(\theta) = \boldsymbol{R}_{i,l}(\theta)\boldsymbol{P}_{l,j,k} + \frac{\vec{s}}{2} \tag{2}$$

where:

$\boldsymbol{I}$ = the matrix of indices, with size $3 \times s_x \times s_z$.

$\boldsymbol{R}_{i,l}\boldsymbol{P}_{l,j,k}$ = the Einstein summation

$$\boldsymbol{R}(\theta) = \begin{bmatrix} \cos\theta & -\sin\theta & 0 \\ \sin\theta & \cos\theta & 0 \\ 0 & 0 & 1 \end{bmatrix}$$

$$\boldsymbol{P}_{i=0} = \begin{bmatrix} -s_x/2 & \cdots & -s_x/2 \\ \vdots & \ddots & \vdots \\ s_x/2 & \cdots & s_x/2 \end{bmatrix}$$

$$\boldsymbol{P}_{i=1} = \boldsymbol{0}_{s_x \times s_z}$$

$$\boldsymbol{P}_{i=2} = \begin{bmatrix} -s_z/2 & \cdots & s_z/2 \\ \vdots & \ddots & \vdots \\ -s_z/2 & \cdots & s_z/2 \end{bmatrix}$$

$$\vec{s} = \begin{bmatrix} s_x \\ s_y \\ s_z \end{bmatrix}$$

A set of images rotated about the depth axis were extracted according to a set of angles $\vec{\theta}_z$, given by Eq. (3).

$$\vec{\theta}_z = \begin{bmatrix} \theta_{z,1} \\ \theta_{z,2} \\ \vdots \\ \theta_{z,n} \end{bmatrix} \tag{3}$$

where:

n = the number of rotations about the z-axis.

$\theta_{z,i} \in [0, 180]$

$i \in [1, 2, \ldots, n]$

2.4. Volume alignment

Since the ultrasound recordings were acquired with minimal inference by the cardiologists, the centerline of the volumetric data did not cut through the true apex of the LV. Thus, 2D images extracted from the volume rotated about the depth axis z contained a shortened LV long-axis and an incorrectly thick apex, a phenomenon known as LV foreshortening. Foreshortening induces underestimation of LV length and volume, and overestimation of global and regional LV function. To minimize the foreshortening in the extracted ultrasound images, the cardiac volume was aligned along the LV by a deep learning-based method, as visualized in Fig. 2.

The proposed method for volume alignment of 3D ultrasound recordings is based on a machine learning model designed to predict numeric values proportional to the length of the LV for a set of images. Since the ultrasound volume is defined within a triangular pyramid shape of 60 degrees in the x- and y-axis, a total of 2 × 60 images rotated about the respective axes were extracted. By feeding the set of images to a 3D convolutional neural network (CNN), the relative length of the ventricle for each image was predicted simultaneously. The x-axis rotational angle θ_x and the y-axis rotational angle θ_y, corresponding to the planes with the longest ventricle, were computed as the peak of the predicted distribution.

The deep neural network architecture adopted for volume alignment in the study was a 3D CNN inception network, given in Fig. 3. The proposed architecture combined convolutions, batch normalization, non-linear activation units, and inception blocks. The second version

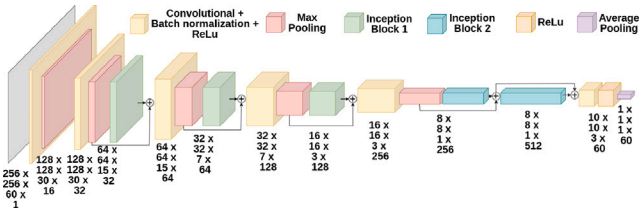

Fig. 3. Visualization of the network for volume alignment, where 'Inception Block 1' indicate a v2 inception block with a (5 × 5) convolution kernel route and 'Inception Block 2' is an identical module without the (5 × 5) convolution kernel route.

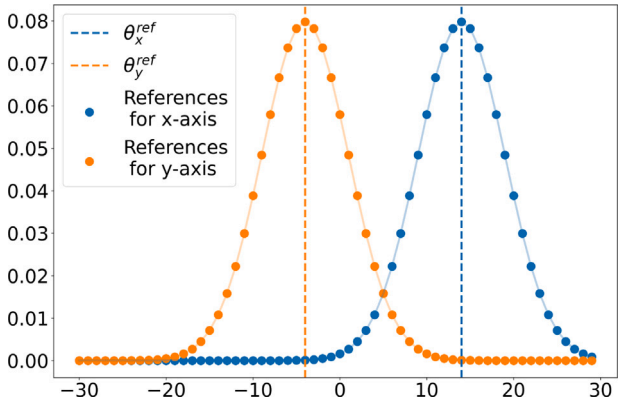

Fig. 4. Illustration of discrete Gaussian distributions used as reference of the LV length for x-axis and y-axis, where $\theta_x^{ref} = 14$ degrees and $\theta_y^{ref} = -6$ degrees.

of the inception blocks, introduced by Szegedy et al. [34], was modified for 3D input and utilized in this network. The model contained comparatively few parameters relative to state-of-the-art networks, which results in a reduced computational cost providing real-time performance.

The CNN was trained as a supervised learning task on the training set of annotated ultrasound images extracted $\vec{\theta}_x$ and $\vec{\theta}_y$ angles about the x- and y-axis. The rotational angle resulting in an image with the longest ventricle and a stationary apex was annotated as θ_x^{ref} for x-axis rotations and θ_y^{ref} for y-axis rotations. A discrete Gaussian distribution with a peak at the annotated θ_x^{ref} and θ_y^{ref} was used as reference throughout training of the CNN. The distribution consisted of 60 numeric values describing the length of the ventricle for the 60 images from the input, where the underlying Gaussian distribution had a standard deviation of 5 degrees, as visualized in Fig. 4.

Estimations of θ_x and θ_y were obtained by the peak of the probability values predicted by the model, with input images rotated about the x- and y-axis, respectively. The volume was aligned by the spatial affine transformation $\boldsymbol{G}$ rotating the volume according to Eq. (4).

$$\boldsymbol{G}(\vec{\theta}, \vec{t}) = \boldsymbol{T}(t_x, t_y, t_z)\boldsymbol{R_y}(\theta_y)\boldsymbol{R_x}(\theta_x)\boldsymbol{T}(t_x, t_y, t_z)^{-1} \tag{4}$$

where:

$\boldsymbol{G}$ = the 4×4 affine transformation matrix

$\boldsymbol{T}$ = the translation matrix

$\vec{t} = \begin{bmatrix} t_x \\ t_y \\ t_z \end{bmatrix}$ is the translation vector

= the 3D coordinates of the probe position.

$\boldsymbol{R}$ = the rotation matrix

$\vec{\theta} = \begin{bmatrix} \theta_x \\ \theta_y \\ 0 \end{bmatrix}$ is the rotation vector.

2.5. Cardiac view classification

To detect the planes corresponding to 2C-, 4C-, or LAX views, a set of 2D images were extracted from the recording after volume alignment. We have defined 2C-, 4C-, and LAX views to be rotated 60 degrees on each other, in line width the guidelines presented by Lang et al. [35]. All three views could therefore be obtained through a prediction of the LAX view, as visualized in Fig. 2. Presuming one single optimal LAX view per volume, most of the extracted 2D images are suboptimal LAX views, or not LAX views at all. Hence, the machine learning model was designed to predict numeric values describing the angular distance of each extracted image plane to the LAX view. The cardiac view classification was in other words resolved as a regression problem by predicting a discrete distribution.

The network adopted for cardiac view classification in the study was a 3D CNN inception network. The proposed network had an identical architecture to the network presented in Fig. 3, but with three times bigger input- and output size. The model was trained by supervised learning on the training set of annotated ultrasound images extracted from 3D TEE recordings, rotated $\vec{\theta}_z$ angles about the depth axis z after volume alignment. The annotated training dataset was a subset of the acquired 3D TEE B-mode ultrasound recordings. The annotation of the rotations corresponding to the LAX view, θ_z^{LAX}, was performed by the first author and corrected by an expert cardiologist. The numeric values describing the angular distance to the LAX view were given by a discrete Gaussian distribution and used as reference during training of the network. The Gaussian distribution had a peak at the annotated θ_z^{LAX} and a standard deviation of 5 degrees.

2.6. Mitral annulus segmentation

A discrete 3D segmentation of the mitral annulus was obtained by detection of the intersection between the annulus and a set of 2D images extracted from all frames of the recordings. To reduce the runtime of the pipeline, images extracted within a region of 30 degrees to θ_z^{2C}, θ_z^{4C} and θ_z^{LAX} and a step degree of 2 were utilized. The CNN obtained by Nordal [18] were applied to predict probability maps of the landmarks on each 2D image.

The probability maps were transformed to coordinate predictions of the landmark in 2D image space by coordinate extraction. The probability maps were converted to binary maps according to Eq. (5), and the center of mass (CoM) of the binary maps resulted in a landmark coordinate and were computed by Eqs. (6) and (7). If the entire binary map was false, the corresponding landmark was discarded in further computations.

$$\hat{b}_{i,j} = \begin{cases} 1, & \text{if } \hat{p}_{i,j} > t \\ 0, & \text{if } \hat{p}_{i,j} \leq t \end{cases} \tag{5}$$

$$CoM_x(\hat{b}) = \frac{1}{N} \sum_{i=1}^{W} \sum_{j=1}^{H} \hat{b}_{i,j}^{x} \tag{6}$$

$$CoM_z(\hat{b}) = \frac{1}{N} \sum_{i=1}^{W} \sum_{j=1}^{H} \hat{b}_{i,j}^{z} \tag{7}$$

where:

$\hat{b}$ = the binary probability map

t = the threshold value

$CoM(\hat{b})$ = the CoM for the binary probability map $\hat{b}$

$\hat{b}_{i,j}^{x}$ = the x-value of the binary probability map at pixel (i,j)

$\hat{b}_{i,j}^{z}$ = the z-value of the binary probability map at pixel (i,j)

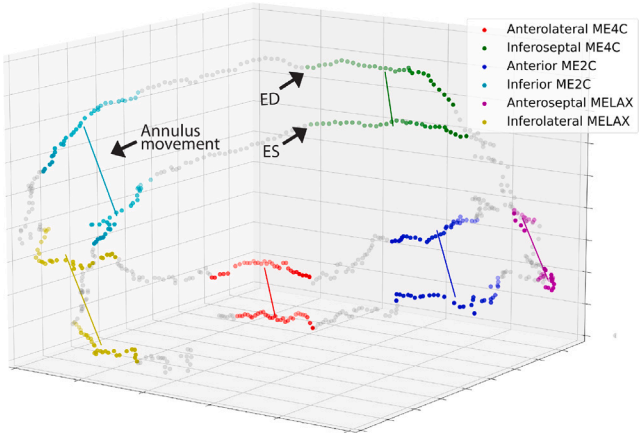

Fig. 5. Visualization of the predicted landmarks in 3D space distributed to the respective cardiac views, at ES and ED. The lines connecting the scattered points indicate the movement of the annulus through the cardiac cycle, related to the MAPSE measure.

The landmark coordinates in image space were transformed to 3D space by the inverse spatial affine transformation $\boldsymbol{H}$. $\boldsymbol{H}$ corresponds to the volume alignment transformation $\boldsymbol{G}$ given in Eq. (4) combined with the basic rotation matrix about the depth axis $\boldsymbol{R}_z(\theta_{z,i})$ related to the extraction of 2D images from the volume. The landmark coordinates in image space were transformed to 3D coordinates according to Eq. (8). Fig. 5 provides a visualization of the predicted mitral annulus landmarks after transformation to 3D space.

$$\vec{l} = \boldsymbol{H}(\vec{\theta}, \vec{t})^{-1} \vec{x} = \boldsymbol{H}(\vec{\theta}, \vec{t})^{-1} \begin{bmatrix} CoM_x \\ 0 \\ CoM_z \\ 1 \end{bmatrix} \tag{8}$$

where:

$\vec{l}$ = the landmark coordinate in $\mathbb{R}^3$

$\boldsymbol{H}(\vec{\theta}, \vec{t}) = \boldsymbol{T}(t_x, t_y, t_z)^{-1} \boldsymbol{R_z}(\theta_z) \boldsymbol{R_y}(\theta_y) \boldsymbol{R_x}(\theta_x) \boldsymbol{T}(t_x, t_y, t_z)$

$\vec{x}$ = landmark coordinates from image space in homogeneous coordinates

$\vec{t} = \begin{bmatrix} t_x \\ t_y \\ t_z \end{bmatrix}$ is the translation vector to the probe position

$\vec{\theta} = \begin{bmatrix} \theta_x \\ \theta_y \\ \theta_z \end{bmatrix}$ is the rotation vector

2.7. Post-processing computations

A set of post-processing computations were applied to obtain MAPSE estimates based on the mitral annulus coordinates in 3D. A subset of the predicted landmarks deviated from the true coordinate due to noise corruption and inaccuracy in the annulus segmentation. The 3D Euclidean distance between all detected landmarks was computed to reject outliers, where all landmarks with an anatomically unfeasible distance to the closest neighbors were discarded. In addition, frame-to-frame jumps of a predicted mitral annulus coordinate of more than 5 mm was considered unphysiological and discarded. If all annulus coordinates of a mitral annular sector were discarded in more than 60% of a cardiac cycle, the respective MAPSE estimate was also discarded.

The MAPSE estimates were calculated by evaluating the excursion of the annulus through the cardiac cycle along a single line of

movement. Since the annulus movement was not perpendicular to the xy-plane, the landmarks were transformed such that the landmark motion was parallel to the z-axis, given by Eq. (9). To obtain the angles of rotation, θ_x and θ_y, the line of best fit to the set of detected 3D landmarks from all frames of the recording was computed. This procedure was completed separately per mitral annular sector. The fitted line was obtained from the unitary matrix of singular value decomposition, and θ_x and θ_y were given by the angle between the line and the x- and y-axis.

$$\boldsymbol{C}(\theta_x, \theta_y, \vec{\hat{c}}) = \boldsymbol{R_y}(\theta_y)\boldsymbol{R_x}(\theta_x)\boldsymbol{T}(\hat{c}_x, \hat{c}_y, \hat{c}_z) \tag{9}$$

where:

$\boldsymbol{C}$ = the rotation correction transformation

θ_x = the rotation about the x-axis

θ_y = the rotation about the y-axis

$\vec{\hat{c}}$ = the end coordinates of the connecting line closest to the probe

$\boldsymbol{R}$ = the rotation matrix about a specified axis

$\boldsymbol{T}$ = the translation matrix

The Euclidean distance between the minimum and the maximum movement of the annulus landmarks after rotation correction was calculated for the CoM of each cardiac cycle of the ultrasound recordings to obtain the MAPSE estimate. The numeric MAPSE estimates were converted from voxel space to the metric system by multiplication of the voxel size correction coefficient.

2.8. Experimental setup

The training of the neural networks was conducted on a computer configuration consisting of an NVIDIA A10-24Q GPU with 23 GB VRAM and 12 Intel® Xeon® Gold 6342 CPU @ 2.80 GHz CPUs. The pipeline was evaluated on the test dataset with an 11th Gen Intel® Core™ i7-11850H @ 2.50 GHz CPU and an NVIDIA RTX A3000 Mobile GPU.

3. Results

3.1. Volume alignment

The training of the network used for volume alignment was completed with a batch size of 6 over 100 epochs. The loss function during the training phase was given by the mean squared error (MSE) between the predicted distribution and the annotated reference Gaussian distribution. The Adam optimizer, introduced by Kingma and Ba [36], was the chosen optimization algorithm in the training of this network and was chosen due to its effectiveness, fast convergence, as well as excellent performance in benchmark tests. A learning rate $\mu = 0.0001$ was chosen for the Adam optimizer, equal to the recommended μ by Kingma and Ba [36]. The three well-established data augmentation techniques, referred to as random rotation, random crop and random flip, were implemented and used in run-time throughout the training of the networks. Additionally, we propose a data augmentation technique designed specifically for the problem at hand. The array of the reference Gaussian distribution, and the corresponding array of input images, was shifted by a random number within the length of the array during training. Such an augmentation ensured that the network learned to identify long-axis images, and avoided a prediction resembling the mean of the training data. The performance metrics from the training of the model is visualized in Fig. 6. The network state at the epoch where the validation loss flattens were saved and used for testing of the method.

Volume alignment was applied on all volumes of the test dataset to estimate the planes with longest ventricle about the x- and y-axis.

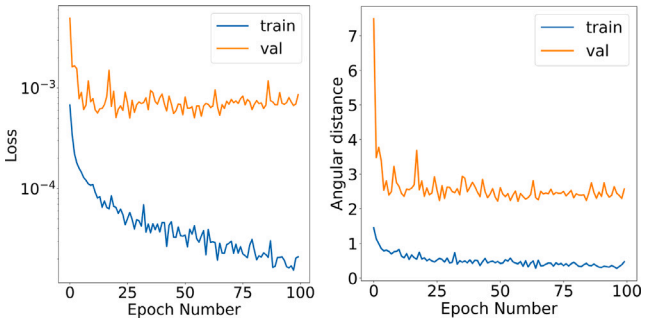

Fig. 6. Performance metrics during training of the volume alignment model. The loss plot indicate the MSE loss, and the plot of angular distance denote the rotational distance from reference- to predicted angle.

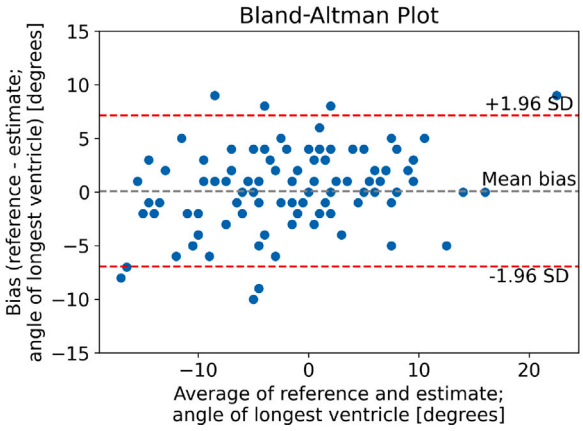

Fig. 7. Bland-Altman plot of agreement of measures between reference and estimated long-axis angle for x- and y-axis rotation.

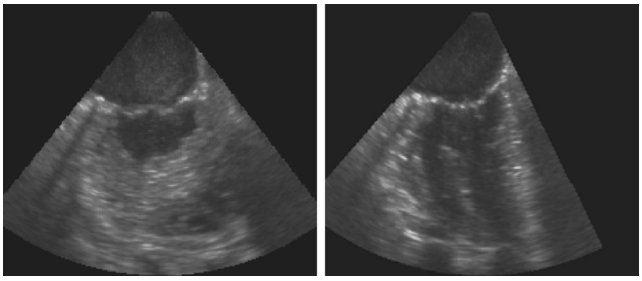

Fig. 8. Example of reduced foreshortening due to volume alignment. The left image represent a 2C view extracted from the raw volume, and the right image is of a 2C view after volume alignment.

The agreement of measures between the estimated and reference long-axis planes is visualized in a Bland-Altman plot, given in Fig. 7. The method achieved a mean difference of (0.09 ± 3.59) degrees compared to reference values.

The alignment of the volume reduced foreshortening in the majority of the acquisitions, confirmed qualitatively through visual inspection of extracted slices by a cardiologist with expertise in echocardiography. Even the worst alignment predictions presented in Fig. 7 resulted in an improved alignment and reduced foreshortening, compared to the unaligned raw volumes. An example of a successful alignment is given in Fig. 8. The complete volume alignment method had an inference time of (2.10 ± 0.34) seconds per recording, including extraction of 120 images of the volume from one frame and alignment estimations by the CNN.

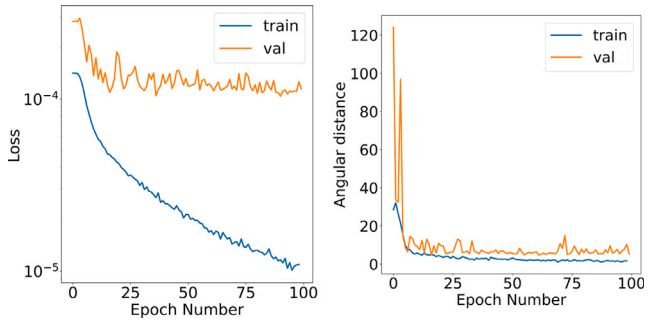

Fig. 9. Performance metrics during training of view classification model. The loss plot indicate the MSE loss, and the plot of angular distance denote the rotational distance from reference- to predicted angle.

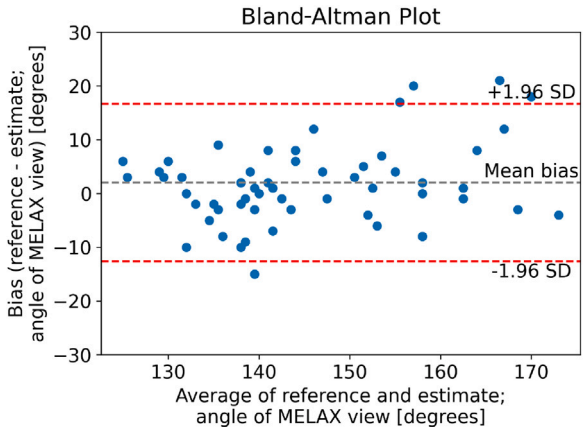

Fig. 10. Bland-Altman plot of agreement of measures between reference and estimated LAX view angle for depth-axis rotation.

3.2. Cardiac view classification

The training of the network used for cardiac view classification was completed with a batch size of 2 over 100 epochs. The distribution predicted by the model were compared to the reference Gaussian distribution by computing the MSE, and functioned as the loss function during the training phase. The estimated θ_z of the LAX view was given by the peak of the predicted distribution. The performance metrics from the training of the model is visualized in Fig. 9. The state of the network was saved at the epoch where the validation loss stagnates, and used later for testing of the method.

The LAX classification pipeline was evaluated on the test dataset by comparison of angular distances between the annotated and estimated LAX view. The proposed method achieved a mean difference of (0.85±6.82) degrees, with an agreement between measures visualized in Fig. 10. The complete LAX classification method had an inference time of (3.17 ± 0.07) seconds per recording, including volume alignment, extraction of 180 images of the volume from one frame and cardiac view classifications by the CNN.

3.3. Mitral annulus segmentation

A discrete segmentation of the mitral annulus was obtained for all recordings in the test dataset. The entire mitral ring was divided into six sectors circumferentially based on the cardiac views. Each sector was covered by 15 2D image slices intersecting with the annulus for every 3D volume in the recording. The landmark detection model predicted the annulus coordinates in the 2D images, and in cases where the predictions resulted in false binary maps, the corresponding landmark was discarded. The number of predicted landmarks per volume for each sector, visualized in Fig. 11, indicates the stability and accuracy of the annulus segmentation. The average number of predicted landmarks out of the maximum possible number of landmark predictions is given in Table 2. The segmentation of the mitral annulus had an inference time of (0.70 ± 0.00) seconds per frame, including volume alignment, extraction of 90 images from the volume, and landmark detections by the CNN.

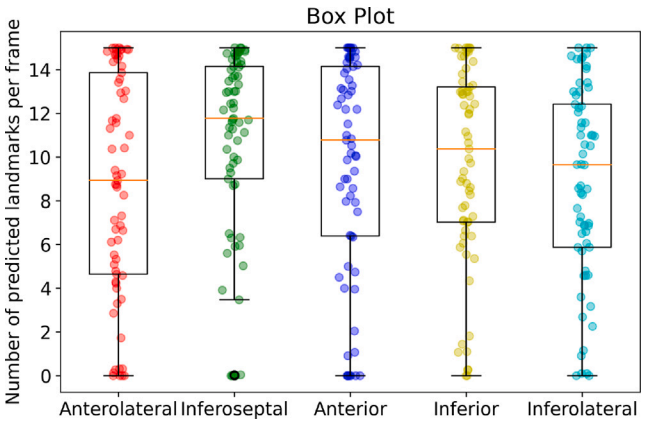

Fig. 11. Box plot of number of predicted mitral annulus landmarks for each mitral annular sector per frame, where 15 is maximum number of landmarks possible to predict.

Table 2
Table of mitral annulus segmentation performance per basal myocardial sector.

Myocardial wall	Average number of predicted landmarks per frame Mean ± SD	Average percentage of predicted landmarks per frame
Anterolateral	9 ± 5	58%
Inferoseptal	11 ± 4	71%
Anterior	10 ± 5	63%
Inferior	10 ± 4	64%
Inferolateral	9 ± 4	58%
All sectors in total	57 ± 22	63%

3.4. MAPSE estimation

The mitral annulus landmark predictions were post processed to reject outliers, and to obtain the mitral plane excursion per cardiac cycle. The post processing pipeline had an inference time of (1.13 ± 1.77) seconds per frame. The pipeline estimated MAPSE parameters in a fully automated manner on the test dataset. MAPSE measures were calculated for the basal myocardial sector of the inferoseptal-, anterolateral-, inferior-, anterior- and inferolateral wall. The five basal myocardial sectors utilized per recording in the test dataset resulted in a total of 310 MAPSE measures. In addition, a global MAPSE estimate was obtained by computation of the mean excursion for the mitral annular sector of the inferoseptal-, anterolateral-, inferior- and anterior wall.

A total of 46 out of the 310 MAPSE reference measures were discarded by the cardiologists with expertise in echocardiography due to unusable image quality. Additionally, 37 MAPSE references were annotated as uncertain due to difficulties with noise at atrium contraction, suboptimal aligned volumes, annulus movement partially out of sector and very low frame rate. The distribution of image quality annotated by the cardiologists is given in Table 3.

The mean difference and standard deviation between automatically estimated MAPSE values and the clinically obtained measures were computed with and without the mitral annular sectors annotated as uncertain. The feasibility of the method is also calculated, describing the method's ability to provide an estimate relative to the measures

Table 3
Table describing the distribution of image quality in the test dataset.

	Available	Including uncertain measures	Exclusively acceptable quality
Number of mitral annular sectors	310	264	227

Table 4
Table of mean difference, standard deviation and feasibility of MAPSE measures between all reference and estimated values.

Myocardial wall	MAPSE estimated mean [mm]	MAPSE md ± sd [mm]	MAPSE feasibility
Anterolateral	8.65 ± 3.52	0.21 ± 1.74	82%
Inferoseptal	8.19 ± 2.94	−0.68 ± 1.66	89%
Anterior	7.15 ± 3.09	−0.62 ± 1.67	82%
Inferior	8.56 ± 2.97	0.01 ± 1.60	74%
Inferolateral	8.63 ± 3.65	−0.75 ± 1.74	64%
Global	8.01 ± 2.71	−0.16 ± 1.06	79%

Table 5
Table of mean difference, standard deviation and feasibility of MAPSE measures between reference and estimated values of acceptable image quality.

Myocardial wall	MAPSE estimated mean [mm]	MAPSE md ± sd [mm]	MAPSE feasibility
Anterolateral	8.93 ± 3.55	0.15 ± 1.78	88%
Inferoseptal	7.88 ± 2.60	−0.63 ± 1.68	94%
Anterior	7.08 ± 2.75	−0.54 ± 1.59	86%
Inferior	8.65 ± 2.96	0.05 ± 1.51	81%
Inferolateral	8.66 ± 3.70	−0.81 ± 1.76	76%
Global	8.08 ± 2.71	−0.13 ± 1.04	87%

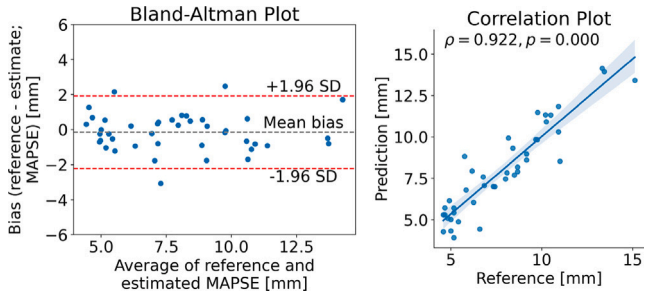

Fig. 12. Bland-Altman and correlation plot of reference and estimated global MAPSE values. Global MAPSE values are computed by the mean of all cardiac cycles in each recording, from 2C- and 4C views. MAPSE references annotated as uncertain are included in this plot.

obtained by the expert cardiologist. Non-feasibility of MAPSE estimates is caused by an insufficient number of predicted annulus coordinates per mitral annular sector, for a given cardiac cycle. Annulus coordinates were discarded if the complete probability map predicted by the CNN was below a threshold value of 60%, as given by Eq. (5). In addition, estimated annulus coordinates with a movement between frames above 5 mm were considered unphysiological and discarded. A MAPSE estimate for a mitral annular sector were discarded if all predicted coordinates were discarded in more than 60% of the respective cardiac cycle.

Table 4 presents the mean difference, standard deviation and feasibility of MAPSE estimates and references, including uncertain measures. Table 5 presents the same statistics, but exclusively for measures with acceptable image quality. The uncertain MAPSE references were excluded to evaluate the effect on feasibility, precision and accuracy.

The difference in measures, including uncertain measures, between the automated estimates and the clinical references is visualized in Figs. 12 and 13, for global and wall-specific MAPSE measures respectively.

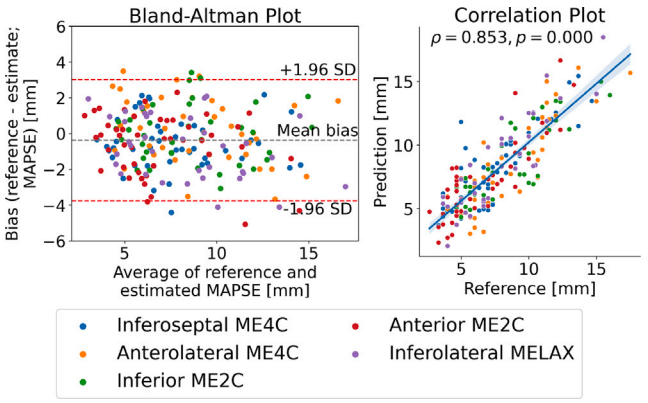

Fig. 13. Bland-Altman plot and correlation plot of reference and estimated MAPSE values per mitral annular sector. Wall-specific MAPSE values are computed by the mean of all cardiac cycles in each recording, for the basal myocardial sector of the inferoseptal-, anterolateral-, inferior-, anterior- and inferolateral wall. MAPSE references annotated as uncertain are included in this plot.

4. Discussion

The MAPSE estimates computed automatically with the proposed method do not show significant systematic errors when compared to clinically obtained reference measures. The mean difference and standard deviation of the estimations equal to (−0.16 ± 1.06) mm is comparable to the inter-observer variability on clinically obtained MAPSE measures on 2D TTE echocardiography [20,37].

The exclusion of ultrasound recordings in the test dataset with borderline image quality had small affect on the mean difference and standard deviation, as presented in Table 5. The feasibility of the method, on the other hand, increased noticeably. This indicates that the method filtered out the MAPSE estimates due to uncertainties in own estimates. In the use case of the method, it is better to avoid uncertain estimates at the cost of feasibility, to limit the number of false predictions. For that reason, the observed behavior of the method is beneficial.

The method for automatic alignment of ultrasound volumes ensures a robust method less dependent on probe positioning and avoidance of foreshortening during acquisition. It is expected that the method handles acquisitions from the OR better with automatic alignment than without, since the movement of the probe and the heart increases in such a setting. As visualized in Fig. 6, the 3D CNN used in volume alignment stagnates after approximately 20 epochs. A similar phenomenon can be observed in Fig. 9, visualizing the performance metrics during the training of the view classification model. To reduce this phenomena, both L1 and L2 regularization of the networks weights were tested. However, such regularization did not affect the stagnation of the loss and were not pursued further. To avoid overfitting the model, the network state at the epoch where the validation loss flattens was used.

The presented method handles 3D ultrasound imagery by slicing the volumes into 2D images. Spatial information related to morphophysiology is lost in such an approach. Direct predictions in 3D with complete volume input in the network architecture might have a positive impact on the predictions. A 3D segmentation of the mitral annulus directly on the ultrasound volume is also beneficial as it removes the need for volume alignment. However, direct volume input in neural networks requires a big dataset for training and validation. Additionally, direct volume inputs are more difficult and computationally more expensive to train. With the available data in this study, such a pipeline was considered unfeasible.

The 3D segmentation of the mitral annulus is based on single-image landmark detection and does not include temporal information

in the predictions. It is expected that the prediction accuracy and precision increase if temporal information from subsequent volumes is introduced to the network architecture. Replacing the single image detection with tracking is recommended for future work.

A potential limitation of the proposed method is the low temporal resolution of 3D TEE ultrasound acquisitions. An average frame rate of 15 can result in underestimations of MAPSE, since the ED and ES may be absent in the recordings. This phenomenon has biggest affect at ED, since the annulus motion is slower at ES. This applies equally to both clinical measures and automatic estimates of MAPSE on 3D data. The absolute value of the MAPSE measurements are consequently lower due to the low temporal resolution. In addition, the agreement between estimated and reference MAPSE measures may be artificially high due to similar reasons. It is expected that underestimations of MAPSE are reduced by computing the average over subsequent cardiac cycles, as it is unlikely that the ED is absent in a set of subsequent cardiac cycles. However, averaging introduces regression toward the mean, which reduces the estimation accuracy. In comparison, 2D ultrasound acquisitions usually have a temporal resolution of above 40 FPS. The big drawback with 2D ultrasound acquisitions is the need for user interaction during acquisition and is thus less suited for fully automatic cardiac monitoring.

It is possible to increase the temporal resolution of ultrasound recordings during the acquisition by adjustment of scanner settings. The frame rate can be adjusted to 25–30 FPS by this approach, hence decreasing the disadvantages of 3D acquisitions. Nevertheless, since such an adjustment is at the expense of spatial resolution, the effects on the precision and accuracy of the method are unknown. There was seemingly no correlation between estimation accuracy and frame rate in the available dataset, but it is recommended to investigate this further in future work. The temporal resolution may also be improved by reducing the acquisition depth. Ultrasound imaging of the entire LV may be unneeded since the mitral annulus is located close to the probe. Thus, a reduced acquisition depth may not decrease the annulus segmentation performance. A reduced depth will, on the other hand, negatively affect the alignment of the volume and might result in a less stable and robust method.

The low frame rate also increases the dependence on stable and accurate mitral annulus segmentation, since outliers have a higher relative impact on the MAPSE estimates. Nevertheless, since the application of the proposed method is in a cardiac monitoring setting, the main interest is intra-patient abrupt changes of the mitral plane excursion. Hence, accurate absolute MAPSE estimates are not as important as detecting the relative change in MAPSE in a perioperative setting. Additionally, it is expected that mean MAPSE estimates from several subsequent cardiac cycles improve the performance and stability of the method, resulting in good enough measures to detect relative changes between different time points throughout a perioperative- and intensive care period.

The proposed method for MAPSE estimation is affected by the movement of the heart during the acquisition since the ultrasound recordings are non-stationary. Respiratory movement is the most common cause of movement and may result in over- or underestimations of MAPSE. The proposed method is only sensitive to movement present during the systole, reducing the influence of movement on the final estimates. There are no indications that this phenomenon has a big impact on the MAPSE estimates in the given dataset. The impact of respiratory movement may also be reduced by the computation of the mean MAPSE through a complete respiratory cycle, which typically equals 5 heart cycles for patients on ventilators. Nevertheless, the impact of heart movement during cardiac surgery might cause a higher estimate variance.

5. Conclusions

This study propose an automated method for functioning and robust non-harming cardiac monitoring of global LV function through MAPSE estimations. A novel pipeline for automatic alignment of ultrasound volumes, automatic classification of 2C-, 4C- and LAX views and automatic 3D segmentation of the mitral annulus were implemented. The excursion of the mitral annulus along the long-axis of the LV were computed to obtain global and wall-specific MAPSE estimates. The proposed method for MAPSE predictions achieved a mean difference of (-0.16 ± 1.06) mm compared to clinical reference measures, which is lower than typical clinical inter-observer variability for MAPSE estimation. The method is fast enough to supplement monitoring in perioperative- and intensive care settings, and may potentially improve the foundation for clinical decision-making.

Declaration of competing interest

- There are no conflict of interests related to the research article, as no private companies funded the research project or was involved in any other way.
- The Norwegian University of Science and Technology (NTNU), Department of Computer Science, was the only funding source of this research project.

Acknowledgments

This work was supported through internal funding by The Department of Computer Science (IDI), Norwegian University of Science and Technology (NTNU).

References

[1] Ponikowski P, Voors AA, Anker SD, Bueno H, Cleland JGF, Coats AJS, Falk V, González-Juanatey JR, Harjola V-P, Jankowska EA, Jessup M, Linde C, Nihoyannopoulos P, Parissis JT, Pieske B, Riley JP, Rosano GMC, Ruilope LM, Ruschitzka F, Rutten FH, van der Meer P, Group ESD. 2016 ESC guidelines for the diagnosis and treatment of acute and chronic heart failure: The task force for the diagnosis and treatment of acute and chronic heart failure of the European Society of Cardiology (ESC)Developed with the special contribution of the Heart Failure Association (HFA) of the ESC. Eur Heart J 2016;37(27):2129–200. http://dx.doi.org/10.1093/eurheartj/ehw128, arXiv:https://academic.oup.com/eurheartj/article-pdf/37/27/2129/23748755/ehw128.pdf.

[2] McDonagh TA, Metra M, Adamo M, Gardner RS, Baumbach A, Böhm M, Burri H, Butler J, Čelutkienė J, Chioncel O, Cleland JGF, Coats AJS, Crespo-Leiro MG, Farmakis D, Gilard M, Heymans S, Hoes AW, Jaarsma T, Jankowska EA, Lainscak M, Lam CSP, Lyon AR, McMurray JJV, Mebazaa A, Mindham R, Muneretto C, Francesco Piepoli M, Price S, Rosano GMC, Ruschitzka F, Kathrine Skibelund A, Group ESD. 2021 ESC guidelines for the diagnosis and treatment of acute and chronic heart failure: Developed by the task force for the diagnosis and treatment of acute and chronic heart failure of the European Society of Cardiology (ESC) with the special contribution of the Heart Failure Association (HFA) of the ESC. Eur Heart J 2021;42(36):3599–726. http://dx.doi.org/10.1093/eurheartj/ehab368, arXiv:https://academic.oup.com/eurheartj/article-pdf/42/36/3599/40594787/ehab368.pdf.

[3] Leichtle SW, Singleton A, Singh M, Griffee MJ, Tobin JM. Transesophageal echocardiography in the evaluation of the trauma patient: A trauma resuscitation transesophageal echocardiography exam. J Crit Care 2017;40:202–6. http://dx.doi.org/10.1016/j.jcrc.2017.04.007.

[4] Borde DP, Joshi S, Asegaonkar B, Apsingkar P, Pande S, More S, Takalkar U, Deodhar A. Mitral annular plane systolic excursion: A simple, reliable echocardiographic parameter to detect left ventricular systolic dysfunction in patients undergoing off-pump coronary artery bypass grafting with transesophageal echocardiography. J Cardiothorac Vasc Anesth 2019;33:1334–9. http://dx.doi.org/10.1053/j.jvca.2018.10.036.

[5] Tempe D. A quick and simple method to reliably assess the left ventricular function with TEE: Is MAPSE the answer? J Cardiothorac Vasc Anesth 2018;33. http://dx.doi.org/10.1053/j.jvca.2018.11.045.

[6] Carlsson M, Ugander M, Mosén H, Buhre T, Arheden H. Atrioventricular plane displacement is the major contributor to left ventricular pumping in healthy adults, athletes, and patients with dilated cardiomyopathy. Am J Physiol - Heart Circ Physiol 2007;292(3):1452–9. http://dx.doi.org/10.1152/ajpheart.01148.2006.

[7] Hensel KO, Roskopf M, Wilke L, Heusch A. Intraobserver and interobserver reproducibility of M-mode and B-mode acquired mitral annular plane systolic excursion (MAPSE) and its dependency on echocardiographic image quality in children. PLoS ONE 2018;13. http://dx.doi.org/10.1371/journal.pone.0196614.

[8] Willenheimer R, Cline C, Erhardt L, Israelsson B. Left ventricular atrioventricular plane displacement: An echocardiographic technique for rapid assessment of prognosis in heart failure. Heart 1997;78(3):230–6. http://dx.doi.org/10.1136/hrt.78.3.230.

[9] Hu K, Liu D, Herrmann S, Niemann M, Gaudron PD, Voelker W, Ertl G, Bijnens B, Weidemann F. Clinical implication of mitral annular plane systolic excursion for patients with cardiovascular disease. Eur Heart J Cardiovascul Imaging 2013;14(3):205–12. http://dx.doi.org/10.1093/ehjci/jes240.

[10] Simonson JS, Schiller NB. Descent of the base of the left ventricle: An echocardiographic index of left ventricular function. J Am Soc Echocardiogr 1989;2(1):25–35.

[11] Borde D, Asegaonkar B, Shreedhar J. Correlation of mitral annular plane systolic excursion (mapse) with left ventricular global longitudinal strain (gls) in patients undergoing coronary artery bypass surgery. J Cardiothorac Vasc Anesth 2021;35:S7–8. http://dx.doi.org/10.1053/j.jvca.2021.08.052, URL: https://www.sciencedirect.com/science/article/pii/S1053077021007254.

[12] Matos J, Kronzon I, Panagopoulos G, Perk G. Mitral annular plane systolic excursion as a surrogate for left ventricular ejection fraction. J Am Soc Echocardiogr 2012;25:969–74. http://dx.doi.org/10.1016/j.echo.2012.06.011.

[13] Alam M. The atrioventricular plane displacement as a means of evaluating left ventricular systolic function in acute myocardial infarction. Clin Cardiol 1991;14(7):588–94. http://dx.doi.org/10.1002/clc.4960140711.

[14] Alam M, Höglund C, Thorstrand C, Philip A. Atrioventricular plane displacement in severe congestive heart failure following dilated cardiomyopathy or myocardial infarction. J Int Med 1990;228(6):569–75. http://dx.doi.org/10.1111/j.1365-2796.1990.tb00281.x.

[15] Magdy G, Hamdy E, Elzawawy T, Ragab M. Value of mitral annular plane systolic excursion in the assessment of contractile reserve in patients with ischemic cardiomyopathy before cardiac revascularization. Indian Heart J 2018;70:373–8. http://dx.doi.org/10.1016/j.ihj.2017.11.004.

[16] Xiao HB, Kaleem S, McCarthy C, Rosen SD. Abnormal regional left ventricular mechanics in treated hypertensive patients with 'normal left ventricular function'. Int J Cardiol 2006;112(3):316–21. http://dx.doi.org/10.1016/j.ijcard.2005.10.001.

[17] Rydberg E, Gudmundsson P, Kennedy L, Erhardt L, Willenheimer R. Left atrioventricular plane displacement but not left ventricular ejection fraction is influenced by the degree of aortic stenosis. Heart 2004;90(10):1151–5. http://dx.doi.org/10.1136/hrt.2003.020628.

[18] Nordal T. Automatic detection of mitral annular plane systolic excursion from transesophageal echocardiography using deep learning (Master's thesis), Norway: Norwegian University of Science and Technology; 2019.

[19] Storve S, Grue JF, Samstad S, Dalen H, Haugen BO, Torp H. Realtime automatic assessment of cardiac function in echocardiography. IEEE Trans Ultrason Ferroelectr Freq Control 2016;63(3):358–68. http://dx.doi.org/10.1109/TUFFC.2016.2518306.

[20] Grue JF, Storve S, Dalen H, Salvesen O, Mjølstad OC, Samstad SO, Torp H, Haugen BO. Automatic measurements of mitral annular plane systolic excursion and velocities to detect left ventricular dysfunction. Ultrasound Med Biol 2018;44(1):168–76.

[21] Orderud F, Torp H, Rabben S. Automatic alignment of standard views in 3D echocardiograms using real-time tracking. In: Progress in biomedical optics and imaging - Proceedings of SPIE 7265. 2009, http://dx.doi.org/10.1117/12.805380.

[22] Veronesi F, Corsi C, Caiani E, Sarti A, Lamberti C. Tracking of left ventricular long axis from real-time three-dimensional echocardiography using optical flow techniques. In: IEEE transactions on information technology in biomedicine : a publication of the IEEE Engineering in Medicine and Biology Society, vol. 10. 2006, p. 174–81. http://dx.doi.org/10.1109/TITB.2005.855535.

[23] Pouch AM, Wang H, Takabe M, Jackson BM, Gorman JH, Gorman RC, Yushkevich PA, Sehgal CM. Fully automatic segmentation of the mitral leaflets in 3D transesophageal echocardiographic images using multi-atlas joint label fusion and deformable medial modeling. Med Image Anal 2014;18(1):118–29. http://dx.doi.org/10.1016/j.media.2013.10.001.

[24] Pedrosa J, Queiros S, Vilaca J, Badano L, D'Hooge J. Fully automatic assessment of mitral valve morphology from 3D transthoracic echocardiography. In: IEEE international ultrasonics symposium, IUS 2018-October. 2018, p. 3–8. http://dx.doi.org/10.1109/ULTSYM.2018.8580112.

[25] Carnahan P, Ginty O, Moore J, Lasso A, Jolley MA, Herz C, Eskandari M, Bainbridge D, Peters TM. Interactive-automatic segmentation and modelling of the mitral valve. LNCS, vol. 11504, Springer International Publishing; 2019, p. 397–404. http://dx.doi.org/10.1007/978-3-030-21949-9_43, arXiv:1905.01344.

[26] Carnahan P, Moore J, Bainbridge D, Eskandari M, Chen EC, Peters TM. Deep-Mitral: Fully automatic 3D echocardiography segmentation for patient specific mitral valve modelling. LNCS, vol. 12905, Springer International Publishing; 2021, p. 459–68. http://dx.doi.org/10.1007/978-3-030-87240-3_44.

[27] Mitral valve annulus localization in 3D echocardiography. In: Proceedings of the annual international conference of the IEEE engineering in medicine and biology society, EMBS 2016-October. IEEE; 2016, p. 1087–90. http://dx.doi.org/10.1109/EMBC.2016.7590892.

[28] Voigt I, Scutaru M, Mansi T, Georgescu B, El-Zehiry N, Houle H, Comaniciu D. Robust live tracking of mitral valve annulus for minimally-invasive intervention guidance. Lecture notes in computer science (including subseries lecture notes in artificial intelligence and lecture notes in bioinformatics), vol. 9349, 2015, p. 439–46. http://dx.doi.org/10.1007/978-3-319-24553-9_54.

[29] Schneider RJ, Perrin DP, Vasilyev NV, Marx GR, Del Nido PJ, Howe RD. Mitral annulus segmentation from 3D ultrasound using graph cuts. IEEE Trans Med Imaging 2010;29(9):1676–87. http://dx.doi.org/10.1109/TMI.2010.2050595.

[30] Schneider RJ, Perrin DP, Vasilyev NV, Marx GR, Del Nido PJ, Howe RD. Mitral annulus segmentation from four-dimensional ultrasound using a valve state predictor and constrained optical flow. Med Image Anal 2012;16(2):497–504. http://dx.doi.org/10.1016/j.media.2011.11.006.

[31] Andreassen BS, Veronesi F, Gerard O, Solberg AH, Samset E. Mitral annulus segmentation using deep learning in 3-D transesophageal echocardiography. IEEE J Biomed Health Inf 2020;24(4):994–1003. http://dx.doi.org/10.1109/JBHI.2019.2959430.

[32] Østvik A, Smistad E, Aase SA, Haugen BO, Lovstakken L. Real-time standard view classification in transthoracic echocardiography using convolutional neural networks. Ultrasound Med Biol 2019;45(2):374–84. http://dx.doi.org/10.1016/j.ultrasmedbio.2018.07.024.

[33] Støylen A, Mølmen HE, Dalen H. Relation between Mitral Annular Plane Systolic Excursion and Global longitudinal strain in normal subjects: The HUNT study. Echocardiography 2018;35(5):603–10. http://dx.doi.org/10.1111/echo.13825, URL: https://onlinelibrary.wiley.com/doi/abs/10.1111/echo.13825.

[34] Szegedy C, Vanhoucke V, Ioffe S, Shlens J, Wojna Z. Rethinking the inception architecture for computer vision. 2015, http://dx.doi.org/10.48550/ARXIV.1512.00567, URL: https://arxiv.org/abs/1512.00567.

[35] Lang RM, Badano LP, Mor-Avi V, Afilalo J, Armstrong A, Ernande L, Flachskampf FA, Foster E, Goldstein SA, Kuznetsova T, Lancellotti P, Muraru D, Picard MH, Rietzschel ER, Rudski L, Spencer KT, Tsang W, Voigt J-U. Recommendations for cardiac chamber quantification by echocardiography in adults: An update from the American society of echocardiography and the European association of cardiovascular imaging. J Am Soc Echocardiogr 2015;28(1):1–39.e14. http://dx.doi.org/10.1016/j.echo.2014.10.003, URL: https://www.sciencedirect.com/science/article/pii/S0894731714007457.

[36] Kingma D, Ba J. Adam: A method for stochastic optimization. In: International conference on learning representations. 2014.

[37] Thorstensen A, Dalen H, Amundsen BH, Aase SA, Stoylen A. Reproducibility in echocardiographic assessment of the left ventricular global and regional function, the HUNT study. Eur J Echocardiogr 2009;11(2):149–56. http://dx.doi.org/10.1093/ejechocard/jep188, arXiv:https://academic.oup.com/ehjcimaging/article-pdf/11/2/149/7137383/jep188.pdf.